

Estimation of the EEG power spectrum using MRI T_2 relaxation time in traumatic brain injury

R.W. Thatcher^{a,b,c,*}, C. Biver^{a,c}, J.F. Gomez^{a,c}, D. North^{a,c}, R. Curtin^{a,c}, R.A. Walker^a, A. Salazar^c

^aBay Pines Veterans Administration Medical Center, Research and Development Service – 151, Bldg 23, Room 117, Bay Pines, FL 33744, USA

^bUniversity of South Florida College of Medicine, Departments of Neurology and Radiology, Tampa, FL, USA

^cDefense and Veterans Head Injury Program, 6825 Georgia Ave., Washington, DC 20307, USA

Accepted 24 May 2001

Abstract

Objectives: To study the relationship between magnetic resonance imaging (MRI) T_2 relaxation time and the power spectrum of the electroencephalogram (EEG) in long-term follow up of traumatic brain injury.

Methods: Nineteen channel quantitative electroencephalograms or qEEG, tests of cognitive function and quantitative MRI T_2 relaxation times (qMRI) were measured in 18 mild to severe closed head injured outpatients 2 months to 4.6 years after injury and 11 normal controls. MRI T_2 and the Laplacian of T_2 were then correlated with the power spectrum of the scalp electrical potentials and current source densities of the qEEG.

Results: qEEG and qMRI T_2 were related by a frequency tuning with maxima in the alpha (8–12 Hz) and the lower EEG frequencies (0.5–5 Hz), which varied as a function of spatial location. The Laplacian of T_2 acted like a spatial–temporal ‘lens’ by increasing the spatial–temporal resolution of correlation between 3-dimensional T_2 and the ear referenced alert but resting spontaneous qEEG.

Conclusions: The severity of traumatic brain injury can be modeled by a linear transfer function that relates the molecular qMRI to qEEG resonant frequencies. © 2001 Elsevier Science Ireland Ltd. All rights reserved.

Keywords: Traumatic brain injury; Magnetic resonance imaging T_2 relaxation time; Entropy; qEEG

1. Introduction

Traumatic brain injury (TBI) occurs when rapid acceleration/deceleration forces are delivered to the skull (Ommaya, 1995; Holbourn, 1943, 1945; Lee and Advani, 1970; Advani et al., 1982; Ommaya et al., 1994). The brain, which is a very energetic 3 pounds of soft tissue, sits inside a bony vault and absorbs the disruptive mechanical energy imparted to the skull causing neural damage and cognitive impairment. Animal studies show that TBI results in disruptions of protein/lipid molecules of the brain at mild levels of force, myelin degeneration at mild to moderate forces and blood disruption at moderate to severe forces (Povlishock and Coburn, 1989; Ommaya, 1968, 1995). In humans, the cognitive consequences of mild TBI are a reduction in the speed and efficiency of cognitive functioning such as in concentration, impaired short-term memory, slowness of thought, depression, problems finding words, reduced attention span, reduced reaction times and psycho-social disor-

ders (Barth et al., 1983; Kwentus et al., 1985; Cronwall and Wrightson, 1980; Rimel et al., 1981).

The quantitative electroencephalogram (qEEG) literature is generally consistent with the neuropsychological literature by showing reduced energy and reduced dynamical complexity of the electroencephalogram (EEG) as a function of the severity of TBI. For example, decreased EEG alpha frequencies and increased delta frequencies are commonly related to the severity of TBI in qEEG studies (Tebano et al., 1988; Mas et al., 1993; von Bierbrauer et al., 1993; Ruijs et al., 1994; Thatcher et al., 1989, 2001; Trudeau et al., 1998). The qEEG literature also shows significant correlations between EEG coherence and EEG phase and TBI in which reduced short distance coherence is most strongly related to the severity of TBI (Thatcher et al., 1989, 1998b, 2001; Hoffman et al., 1995, 1996; Trudeau et al., 1998; Thornton, 1999). Finally, the qEEG and the quantitative MRI (qMRI) are conjointly related to the severity of TBI and cognitive dysfunction in studies showing shifts in T_2 relaxation time related to the severity of injury and the EEG power spectrum (Thatcher et al., 1997, 1998a,b, 2000).

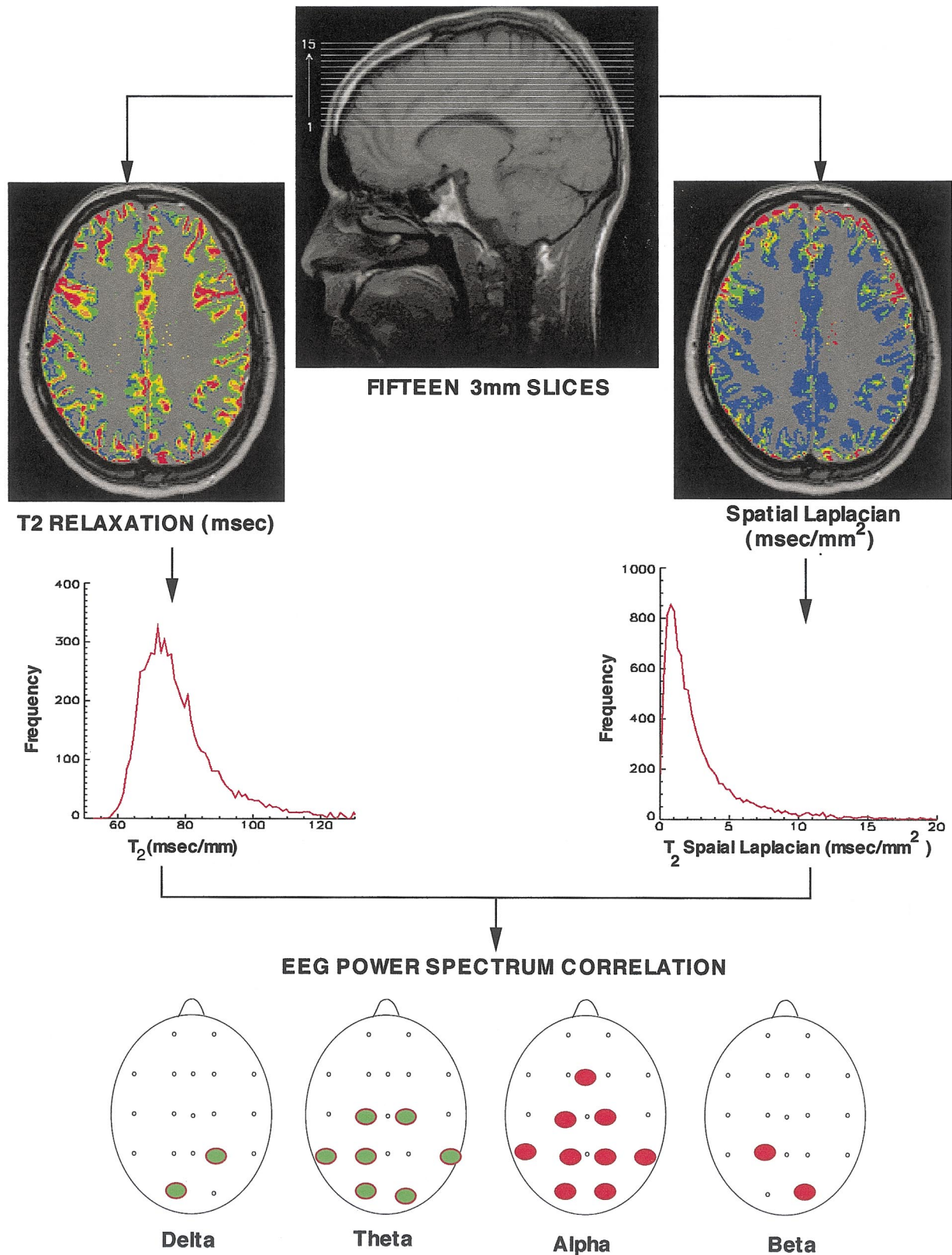
An important unanswered question is to what extent can

* Corresponding author. Fax: +1-727-391-0890.

E-mail address: bobt2@gte.net (R.W. Thatcher).

T_2 relaxation time provide a quantitative measure of spatial biophysical differences and biophysical complexity within the brain? Another related question concerns the possible

clinical relevance of quantitative T_2 relaxation time as a measure of biophysical complexity in normal subjects vs. traumatic brain injured patients. Whittall et al. (1997)



presented quantitative T_2 relaxation time analyses of the brains of normal subjects in which the posterior internal capsule and splenium of the corpus callosum exhibited shorter T_2 relaxation times than in other white matter brain regions. It is notable that the quantitative differences in T_2 relaxation time were not visually discernible on conventional magnetic resonance (MR) images (Whittall et al., 1997). Studies by Tillman et al. (1997) also revealed spatial heterogeneities in T_2 relaxation times in normal and schizophrenic patients. Spatial heterogeneities in T_2 relaxation times have also been used to quantify myelin development (Miot-Norault et al., 1997).

The purpose of the present study is to more deeply investigate the relationship between qEEG and qMRI in TBI by focusing on the relationship between spatial complexity of T_2 relaxation time and the EEG power spectrum. This will be done by correlating the 3-dimensional spatial Laplacian of T_2 relaxation time with the scalp EEG electrical potential and the estimated EEG current source density (CSD). A secondary goal of this study is to determine whether or not the spatial Laplacian equation in general is a useful concept for the unification of qEEG and qMRI.

2. Methods

2.1. Closed head injured patients

Eighteen closed head injured and TBI patients were included in this study (17 males and one female who ranged in age from 19 to 48 years, mean age = 32.6 years, SD = 10.6 years). The patients only suffered closed traumatic brain injuries and had a range of severity from mild to severe. All of the patients were in the chronic or non-acute post-injury edema condition (time from injury to EEG and MRI evaluation ranged from 20 days to 6 years with a mean of 1.7 years between injury and EEG/MRI test). The time interval between the qEEG and the MRI test ranged from 2 h to 4 days. The severity of injury varied from moderate to severe, but all of the subjects were conscious and alert with varying amounts of completed rehabilitation at the time of testing. The patients were tested as part of a Defense and Veterans Head Injury Program (DVHIP). Approximately 66% of the subjects were motor-vehicle accident (MVA) victims, 17% were victims of industrial or home accidents and 17% were victims of violent crime.

2.2. Normal control subjects

A total of 11 male neurologically normal high school students, ranging in age from 13.96 to 17.68 years (mean = 16.12 years and SD = 1.74 years), were also included in this study. The control subjects were recruited from local high schools in the San Diego area as part of a DVHIP pilot project to study the effects of football concussions on cognitive and neurological functions (Daniel et al., 1999). The MRI and EEG data were obtained during the pre-season period, prior to the football season.

2.3. MRI acquisition

The MR images from the TBI patients were acquired on a 1.5 T Picker scanner located at the Tampa James A. Haley VA Medical Center and the normal control subjects MRI were acquired on a 1.5 T GE scanner at the California Balboa Naval Medical Center. The same exact acquisition sequences were used on both MRI machines. The acquisition for both groups of subjects was a 3 mm slice thickness and no gap sequences using a conventional spin-echo sequence. The proton density (PD) and T_2 sequences acquired as a interleaved double echo with a repetition time (TR) of 3000 ms and echo times (TEs) of 30 and 90 ms, field of view (FOV) of 24 cm, a 90° flip angle and a 256 × 256 matrix. The T_1 -weighted sequence used TR = 883 ms with TE = 20 ms, FOV = 24 cm, a 90° flip angle and a 256 × 256 matrix.

2.4. Segmentation and slice selection

The goal was to estimate the neocortical gray matter T_2 relaxation time in each pixel. We used a multispectral (i.e. T_1 , T_2 and PD) k -Nearest Neighbor (kNN) and fuzzy c -means algorithm for gray matter, white matter and cerebrospinal fluid (CSF) segmentation (Clarke et al., 1995; Bezdek et al., 1993; Bensaid et al., 1994). The volumes of gray matter in this study were primarily neocortical in origin. Slices 1–15 begin from the starting slice above the thalamus and basal ganglia near the middle temporal lobes and extend to approximately 1.5 cm from the bottom of the skull (Thatcher et al., 1997, 1998a,b). Fig. 1 (top) illustrates the location and orientation of the gray matter volume in this study.

Fig. 1. Diagram of the MRI and EEG experimental design. Top center shows the location of the fifteen 3 mm MRI slices (Thatcher et al., 1997, 1998a,b). Top left is an example of a T_2 relaxation time map from the segmented gray matter showing the distribution of T_2 relaxation times in a given slice. T_2 relaxation time is represented in pseudocolor where blue = 62–69 ms, green = 69–77 ms, yellow = 77–84 ms, orange = 84–92 ms and red \geq 92 ms. Top right is an example of a spatial Laplacian T_2 relaxation time map from the segmented gray matter showing the distribution of the second spatial derivative of T_2 relaxation times in a given slice. The second spatial derivative of T_2 relaxation time is represented in pseudocolor where blue = 0–5 ms/mm², green = 5–9 ms/mm², yellow = 9–15 ms/mm², orange = 15–20 ms/mm² and red \geq 20 ms/mm². Middle row left is the T_2 relaxation time histograms from the gray matter and right is the histogram of the second spatial derivative of T_2 relaxation time. The bottom row shows the location of the 19 scalp electrodes and diagrammatically illustrates the correlation between the second spatial derivative of T_2 relaxation time and the EEG power spectrum. The red circles represent positive correlations between the EEG frequency band and the spatial Laplacian of T_2 relaxation time and the green circles represent negative correlations. These are only illustrations of the experimental design.

2.5. Calculations of MRI T_2 relaxation times

We used the conventional two-point solution of the Bloch equations (Bloch, 1946) to calculate T_2 relaxation time (Dixon and Ekstrand, 1982; Kjos et al., 1985; Darwin et al., 1986; Hickley et al., 1986; Mills et al., 1984). According to this solution, MR signal intensity (I) is related to proton relaxation times by: $I = KN(1 - e^{-(TR/T_1)}) e^{-(TE/T_2)}$ where K is velocity and scaling constants, N the hydrogen spin density, TR the repetition time, TE the echo time, T_1 the spin–lattice relaxation time and T_2 the spin–spin relaxation time. T_2 was solved analytically using the PD and T_2 images acquired in an interleaved manner where the corresponding TR values were equal, $TR \gg TE$ and molecular velocity and scaling is 1. The equation was

$$T_2 = \frac{(TE_{PD} - TE_{T_2})}{\ln(I_{T_2}/I_{PD})}$$

where I_{T_2} and I_{PD} were the pixel intensities from the respective T_2 and PD images. In this manner, T_2 relaxation time was computed for each pixel in each slice (Thatcher et al., 1998a,b, 2000).

2.6. Second spatial derivatives of T_2 relaxation times

Each 3 mm MRI slice is a $24 \times 24 \text{ cm}^2$ rectangular matrix of 256 columns by 256 rows of T_2 relaxation time voxels each of a dimension of $0.94 \times 0.94 \text{ mm}^2$ per pixel (based on the field of view and the matrix size). The Savitzky–Golay procedure was used (Press et al., 1994) to compute the spatial derivative in an array of 256 pixels, which involved fitting a second order polynomial (width = 5) and then numerically evaluating the polynomial to compute the second derivative. The value of the derivative is the Savitzky–Golay convolution divided by the sampling interval (or 0.94 mm). The mean of the approximately 6000 gray matter second derivative values in a 3 mm slice was the independent variable and the EEG as the dependent variable in this study. Edge effects, such as the boundaries between skull, CSF and white matter were minimized by the segmentation procedure described in Section 2.4. Edge effects due to field inhomogeneities with CSF were minimized by selecting slices that were above the ventricles and primarily contained the gray matter of the neocortex. This resulted in an approximately normal distribution of T_2 values and a typically skewed second derivative as shown in Fig. 1.

2.7. 3-Dimensional vector representation of T_2 relaxation time

As described in Section 2.6, the Savitzky–Golay procedure (Savitzky and Golay, 1964) was used to compute the second derivatives in the x and y directions within a slice (i.e. vector length = 254 (i.e. $256 - 2$ for the second derivative) in the x direction and 254 in the y direction). The slice thickness was 3 mm and, therefore, a linear interpolation in the z direction across 3 mm slices was conducted in

order to scale the between slice second spatial derivatives to the within slice dimensions of $0.94 \times 0.94 \text{ mm}^2$ and 256 equally spaced points. The z direction vector was then smoothed using the same Savitzky–Golay parameters (Press et al., 1994) and the second derivative numerically evaluated as described previously. This procedure produced a 3-dimensional spatial derivative for each T_2 relaxation time voxel in the x , y and z directions in which the second derivative as the local spatial Laplacian in ms/mm^2 .

The 3-dimensional T_2 Laplacian operator is mathematically defined as:

$$\frac{\partial^2 T_2}{\partial x^2} + \frac{\partial^2 T_2}{\partial y^2} + \frac{\partial^2 T_2}{\partial z^2} = \nabla^2 T_2$$

i.e. as the second order partial derivatives of the 3-dimensional T_2 spatial gradients. T_2 is a scalar quantity similar to temperature, with gradients of difference in the scalar values. The Laplacian is a measure of the second order rate of change of T_2 relaxation time in the vicinity of each voxel. This analysis provided a 3-dimensional second derivative spatial measure at each T_2 relaxation time voxel as defined by the magnitude of the resultant vector for each T_2 relaxation time gray matter voxel, as represented in spherical coordinates.

According to this formulation, T_2 relaxation time is a scalar, located in a 3-dimensional space as defined by the coordinates of the MRI. The second derivative of any 3-dimensional vector array of numbers is equal to 0 if the neighboring space is smooth and unchanging. The Laplacian was computed from the 256×256 vectors of MRI intensities, which contained gray matter, white matter and CSF. Edge effects of the Laplacian were minimized by only using the mean of the distribution of Laplacian values from the selection of gray matter pixels located in the interior of the brain and above the ventricles.

The selection of the first axial slice was the same for all patients and normals. Fig. 1 (top) shows the lowest and starting slice which was identified at the level of the genu of the corpus callosum, septum pellucidum and the forceps major and minor (Thatcher et al., 1997, 1998a,b, 2000).

Histograms of the T_2 measures were plotted and outliers ≥ 4 standard deviations were removed before computing means and modes. This procedure further eliminated any spikes or edge effects that may be present in the Laplacian. Whole slice means, modes and standard deviations were computed for the first and second derivative resultant magnitudes and angles of T_2 relaxation time for the cortical gray matter. Only the results of the average magnitudes of gray matter T_2 relaxation times and the average magnitudes of gray matter spatial second derivative are presented in this paper.

2.8. Experimental design

Fig. 1 shows the experimental design in which each MRI slice was segmented into gray and white matter and CSF and the mean of T_2 relaxation time and the second spatial derivative

vative (i.e. the Laplacian) were calculated only for the segmented neocortical gray matter. The frequency distribution of T_2 relaxation time values in a 3 mm slice of the neocortical gray matter is shown on the left middle row of Fig. 1 and the frequency distribution of the second spatial derivative of that same gray matter slice is shown on the right middle row of Fig. 1. The gray matter mean T_2 relaxation time and the mean resultant magnitude of the 3-dimensional Laplacian were calculated for each slice for each subject. This yielded 15 mean T_2 relaxometry measures, 15 T_2 Laplacian measures and 4 EEG frequencies at each of the 19 electrode locations per subject.

2.9. EEG recording

Power spectral analysis was implemented on 3–5 min segments of eyes closed resting EEG recorded from 38

scalp locations using the left ear lobe as a reference in the TBI patients and normal controls. Only the results of the 19 channel 10/20 EEG locations is reported in this paper. EKG and eye movement electrodes were applied to monitor artifact and all EEG records were edited to remove any visible artifact. The amplifier bandwidths were nominally 0.5–30 Hz, the outputs being 9 db down at these frequencies. Three to 5 min of eyes closed EEG was digitized at 128 Hz and spectrally analyzed using complex demodulation (Otnes and Enochson, 1972). The edited EEG epoch length for the complex demodulation varied from 49.5 to 125 s (mean = 87 s). The complex demodulation of the absolute EEG amplitude was computed from the 19 scalp locations in the delta (0.5–3.5 Hz), theta (3.5–7 Hz), alpha (7.5–13 Hz), and beta (13–22 Hz) frequency bands. The frequency bands, including the center frequencies (f_c) and one-half power values (B) were delta (0.5–3.5 Hz;

Correlations: MRI - T2 Gray Matter with EEG - Relative Power

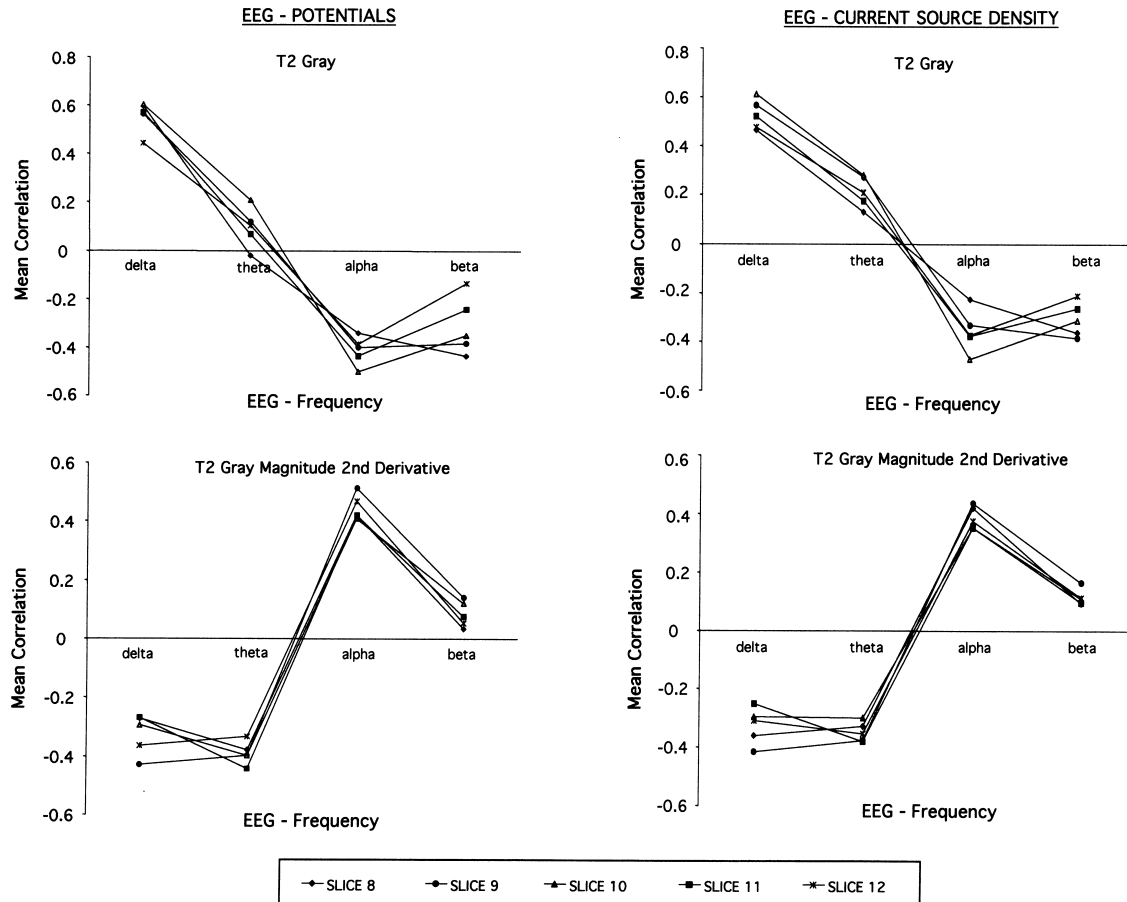


Fig. 2. Mean correlations between T_2 and EEG frequency in TBI patients. The left column are mean correlations between EEG potentials and T_2 relaxometry and the right column are the mean correlations between EEG CSD and T_2 relaxometry. The top row are correlations between EEG frequency and T_2 relaxation time and the bottom row are correlations between EEG frequency and the spatial Laplacian of T_2 relaxation time. The opposite relationship between T_2 relaxation time and the spatial Laplacian of T_2 and EEG frequency is seen by comparing the top row to the bottom row. No difference in the mean correlations were present between the EEG potentials and the EEG CSD which is seen by comparing the left vs. right column. Increased T_2 relaxation time was correlated with increased delta and decreased alpha EEG frequencies. The spatial Laplacian of T_2 relaxation time showed a positive correlation with EEG alpha and a negative correlation with delta and theta frequency bands.

$f_c = 2.0$ Hz; and $B = 1.0$), theta (3.5–7.0 Hz; $f_c = 4.25$ Hz; and $B = 3.5$ Hz), alpha (7.0–13.0 Hz; $f_c = 9.0$ Hz; and $B = 6.0$ Hz), beta (13–22 Hz; $f_c = 19$ Hz; and $B = 14.0$ Hz). EEG amplitude was computed as the square root of power. Relative power was computed by dividing the sum of the power into the power within a given frequency band. The mathematical details of the analyses are provided in Otnes and Enochson (1978).

2.10. Estimates of EEG current source density

The spherical harmonic Fourier expansion (SHE) of the EEG scalp potentials was used to compute the surface Laplacian and thus the CSD at each scalp location (Pascual-Marqui et al., 1988). As pointed out and cross-validated by Pascual-Marqui et al. (1988), the EEG CSD is the second spatial derivative or Laplacian of the scalp electrical potentials.

3. Results

3.1. Correlations between T_2 relaxation time and the power spectrum of EEG potentials and current source density

Fig. 2 shows the mean correlation between EEG potentials (left column) and EEG CSD (right column) from the C3 electrode with T_2 relaxation time in the upper MRI slices in the top row and the T_2 Laplacian in the bottom row. Examination of the columns in Fig. 2 shows that the EEG potentials and the EEG CSD yield very similar correlations to T_2 relaxation time and to the T_2 spatial Laplacian. However, examination of the rows in Fig. 2 shows a clear difference in the mean correlation to EEG frequency between T_2 relaxation time and the neocortical T_2 spatial Laplacian for both the EEG potentials and the CSD. For example, in Fig. 2, lengthened T_2 relaxation times were correlated with increased delta activity and decreased alpha activity. In contrast, the T_2 second spatial derivative was oppositely correlated to the alpha EEG frequency band and the delta and theta frequency bands. Age and time from injury to EEG or MRI test were not significantly correlated to either the EEG relative power or the T_2 relaxation times.

Table 1 shows the results of analyses of variance (ANOVA) using the correlation between T_2 mean relaxation time and EEG frequency for both the electrical potentials and CSD as the factors. Table 1 shows that statistically significant decreases in alpha and beta frequency relative power and significant increases in delta and theta EEG relative power were correlated with increased mean T_2 relaxation time. Both the EEG potentials and the EEG CSD were statistically related to T_2 relaxation time with no significant difference between CSD and the EEG potentials.

Table 2 shows the results of ANOVA using the correlation between second spatial derivative or Laplacian of T_2 relaxation time and EEG frequency in relative power as the factors. Table 2 shows that statistically significant

Table 1
 T_2 relaxation time and the EEG power spectrum

| EEG frequency band | EEG relative power | EEG CSD |
|--------------------|--------------------------|---------------------------|
| Delta (0.5–4 Hz) | $t = 8.876; P < 0.0001$ | $t = 35.70; P < 0.0001$ |
| Theta (4–7 Hz) | $t = 8.529; P < 0.0001$ | $t = 14.41; P < 0.0001$ |
| Alpha (7–13 Hz) | $t = -9.276; P < 0.0001$ | $t = -126.31; P < 0.0001$ |
| Beta (13–22 Hz) | $t = 2.421; P < 0.016$ | $t = -23.80; P < 0.0001$ |

increases in alpha and beta frequency relative power and significant decreases in delta and theta EEG relative power were correlated with increasing T_2 spatial Laplacian values. Age and time from injury to EEG or MRI test were not significantly correlated to either the EEG CSD or the Laplacian of T_2 relaxation times.

Fig. 3 shows representative scattergrams of the relationship between EEG CSD in the alpha band and T_2 relaxation time on the left and the second spatial derivative of T_2 on the right. It can be seen that T_2 relaxation time and the second spatial derivative of T_2 exhibit opposite relationships to the EEG power spectrum. In general, all of the statistically significant scattergrams were well behaved and exhibited a linear relationship between T_2 relaxation time and/or the second spatial derivative of T_2 relaxation time and the EEG.

3.2. Scalp spatial frequency differences between T_2 relaxation and the T_2 second spatial derivative

Fig. 4(A) shows the slice by slice topographic distribution of statistically significant mean correlations between T_2 relaxation time and EEG relative power for 19 scalp leads from slices 1 to 15 (i.e. approximately 3 mm to 4.5 cm below the dura surface). The correlations between T_2 relaxation times and the power spectrum of the EEG potentials and the EEG CSD were the same as for the ear referenced electrical potentials, which were relatively equal for the left and right hemisphere and slightly more prominent in the frontal regions than in the posterior scalp regions.

Fig. 4(B) shows the same slice by slice topographic representation of statistically significant correlations between the second spatial derivative of T_2 relaxation time and EEG relative power. It can be seen that the correlations between the spatial Laplacian of T_2 relaxation times and the EEG power spectrum were more localized to the upper MRI slices and more localized to the central, parietal and occipital scalp regions than were the correlations to T_2 relaxation

Table 2
Spatial Laplacian of T_2 relaxation time and the EEG power spectrum

| EEG frequency band | EEG relative power | EEG CSD |
|--------------------|--------------------------|--------------------------|
| Delta (0.5–4 Hz) | $t = -10.44; P < 0.0001$ | $t = -9.42; P < 0.0001$ |
| Theta (4–7 Hz) | $t = -20.06; P < 0.0001$ | $t = -16.54; P < 0.0001$ |
| Alpha (7–13 Hz) | $t = 19.10; P < 0.0001$ | $t = 16.49; P < 0.0001$ |
| Beta (13–22 Hz) | $t = 11.40; P < 0.0001$ | $t = 9.472; P < 0.0001$ |

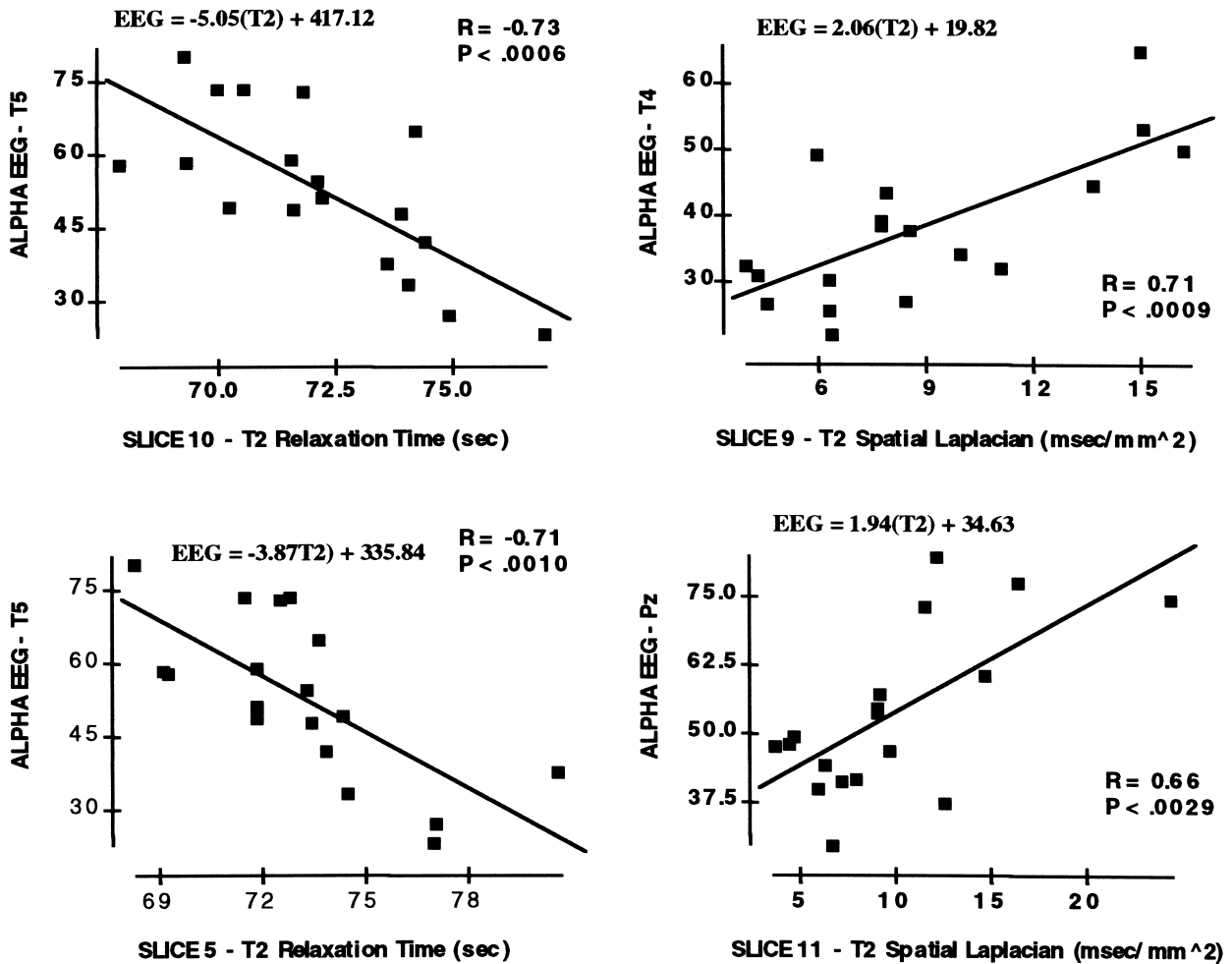


Fig. 3. Representative scattergrams in TBI patients. The left column are scattergrams between EEG relative power and T_2 relaxation time in the alpha frequency band. The right column are scattergrams between EEG relative power and the spatial Laplacian of T_2 relaxation time in the same EEG leads and the same alpha frequency band as on the right. In general, the opposite direction of relationship between EEG power and T_2 relaxometry is seen depending on whether one uses T_2 relaxation time or the second spatial derivative of T_2 relaxation time.

time itself. This same increased spatial resolution in the correlation between the spatial Laplacian of T_2 was present for EEG CSD.

3.3. Correlations between age, neuropsychological performance and T_2 relaxation time

Table 3 shows the results of ANOVA for different neuropsychological tests using MRI slices as factors for both T_2 relaxation time and the T_2 spatial second derivative. No statistically significant correlation with age or time from injury to EEG recording was present. However, statistically significant relations were observed between cognitive functioning and MRI relaxometry in which the longer the T_2 relaxation time and/or the smaller the T_2 spatial second derivative, lower was cognitive functioning. The T_2 second spatial derivative was slightly stronger in its relationship to cognitive functioning in comparison to T_2 relaxation time itself. Fig. 5 shows representative scattergrams between

cognitive functioning and T_2 relaxometry in which the direction of the correlation is the opposite for T_2 vs. the second spatial derivative of T_2 . Because many different neuropsychological tests were significantly related to T_2 relaxation time, no comparative analyses were conducted. In general, the upper MRI slices were more significantly related to cognitive functioning than the lower slices.

3.4. Correlations between neuropsychological performance and EEG current source density

Table 4 shows the results of ANOVA for different neuropsychological tests using EEG relative power and CSD at different frequencies as factors. Statistically significant relations were observed between cognitive functioning and the EEG power spectrum in which the higher frequencies (alpha and beta) were correlated with higher cognitive performance while the lower EEG frequencies were correlated with lower cognitive functioning. The EEG appeared

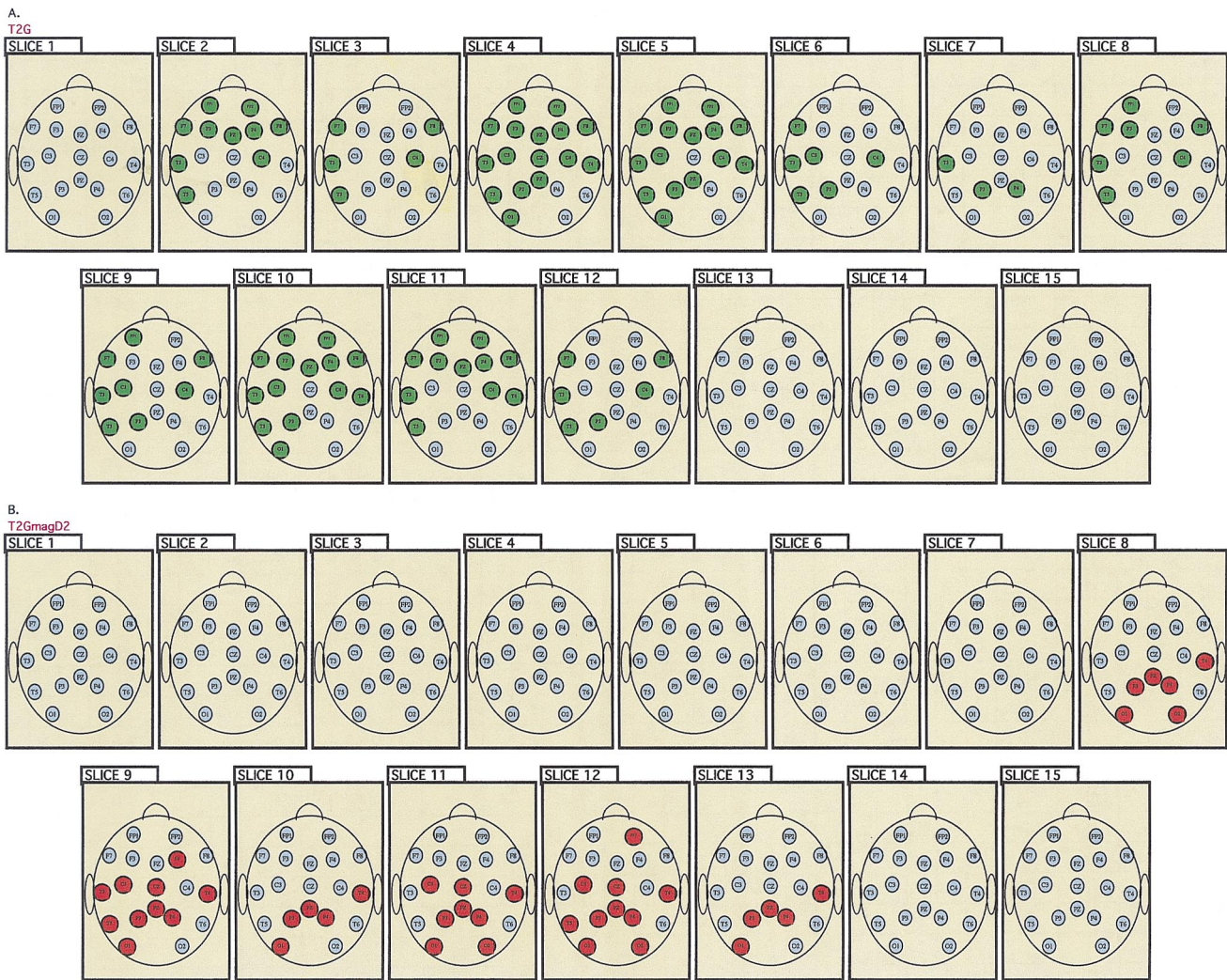


Fig. 4. Topographic distribution of correlations between T_2 relaxometry and EEG alpha relative power. The top two rows (A) are the slice by slice topographic distribution of statistically significant mean correlations between T_2 relaxation time and EEG relative power in the alpha frequency band for 19 scalp leads from slice 1 to slice 15 (i.e. approximately 3 mm to 4.5 cm below the dura surface). The bottom two rows (B) are the slice by slice topographic distribution of statistically significant mean correlations between spatial Laplacian of T_2 relaxation time and EEG relative power in the alpha frequency band for 19 scalp leads from slice 1 to slice 15. It can be seen that the correlations between the spatial Laplacian of T_2 relaxation times and the EEG alpha power were more localized to the upper MRI slices and more localized to the central, parietal and occipital scalp regions than were the correlations to T_2 relaxation time itself. Red color is negative correlation $P < 0.01$ and green color is positive correlation $P < 0.01$.

to be slightly weaker in its correlation with cognitive performance than was the T_2 MRI relaxometry measures.

3.5. Correlations between the EEG power spectrum and MRI relaxometry in normal control subjects

Fig. 6 shows representative scattergrams between T_2 relaxometry and EEG frequency in the normal control subjects similar to what was observed for the TBI patients (see Fig. 1). The second spatial derivative was more statistically significant than the T_2 relaxation time itself and the lower slices tended to be more significant than the upper slices. Statistically significant EEG– T_2 correlations with normal patients were localized to one or two lower slices and overall showed a weaker correlation to EEG than did

Table 3
MRI relaxometry and cognitive function^a

| NeuroPsych test | T_2 Relaxation time (P value) | T_2 spatial Laplacian (P value) |
|-----------------------|---------------------------------------|---|
| WAIS | <0.012 | <0.0001 |
| COWA | <0.0001 | <0.0001 |
| Trail making | NS | NS |
| WISC card sort | NS | NS |
| Wechsler memory scale | NS | <0.0003 |
| CVLT | NS | NS |
| Sternberg | NS | NS |
| VSPL | NS | <0.0001 |

^a WAIS, Wechsler Adult Intelligence Scale; COWA, Controlled Oral Word Association; CVLT, California Verbal Learning Test; VSPL, Visual Spatial Learning Test.

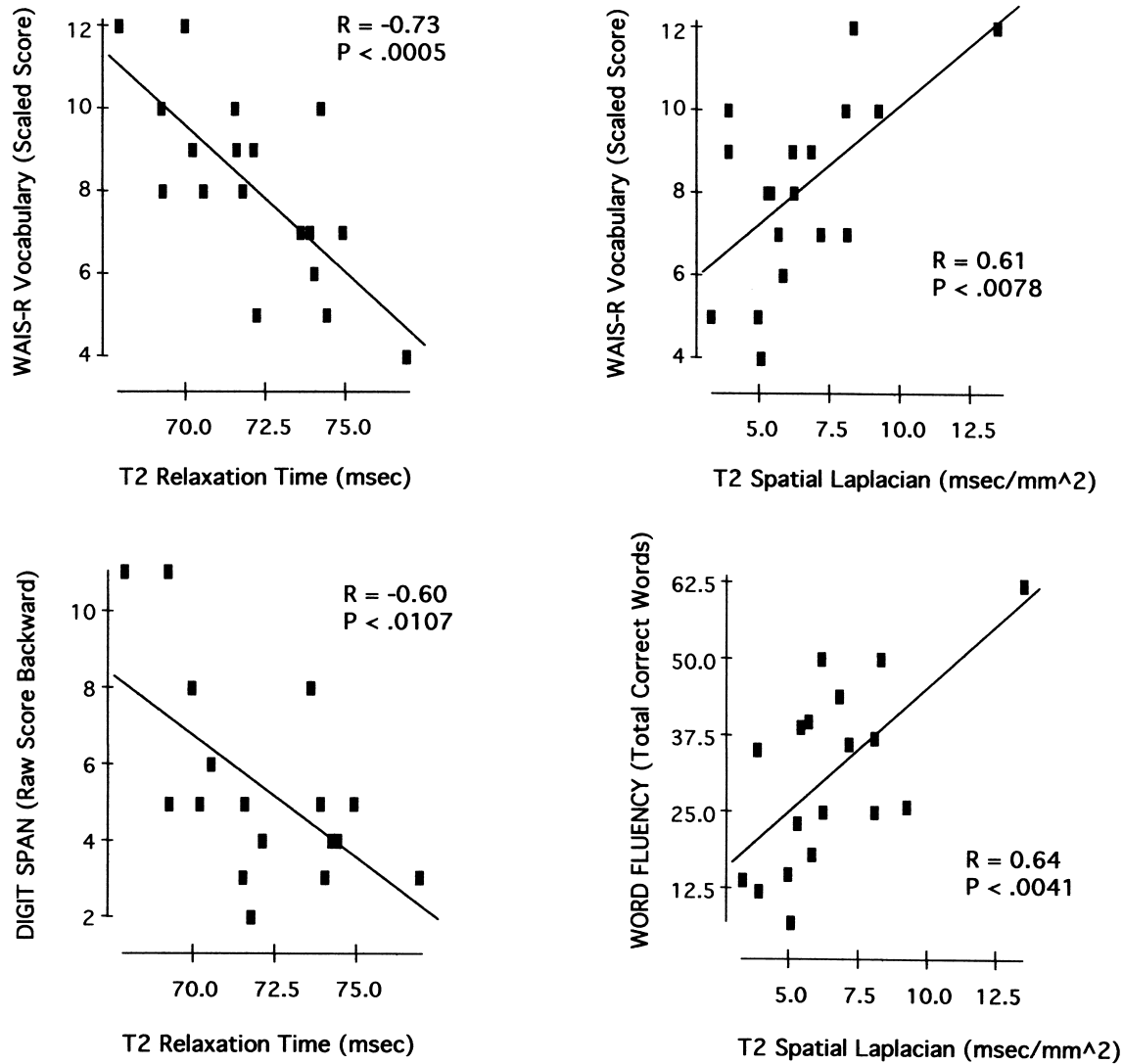


Fig. 5. Scattergrams and correlations between neuropsychological performance and T_2 relaxometry. The left column are representative scattergrams between different neuropsychological tests and T_2 relaxation time. The right column are representative examples of scattergrams for the same neuropsychological tests using the spatial Laplacian of T_2 relaxation time. Opposite directions of correlation between T_2 relaxation time and the spatial Laplacian of T_2 relaxation time were consistently present, similar to the opposite direction of correlation between these two measures of relaxometry and the EEG (Figs. 2 and 3).

the TBI patients. Fig. 7 illustrates the difference in the strength of correlation between T_2 and EEG in normal subjects vs. the TBI patients. The largest differences between normal subjects and TBI patients were in the delta and alpha frequencies in which normal subjects failed to show a statistically significant correlation.

4. Discussion

The results of this study demonstrate a statistically significant linear relationship between 3-dimensional T_2 relaxation time and the human scalp-recorded EEG. A linear qEEG relationship between T_2 and qEEG was observed with respect to a ear reference as well as for the spatial Laplacian of the qEEG or the 'reference free' CSD (Fig.

2). T_2 and the spatial Laplacian of T_2 was most significantly related to the EEG alpha frequency in which a type of resonance or frequency tuning was observed (Fig. 2 and Table 1). In general, the longer the T_2 relaxation time the lower is the magnitude of EEG alpha power (Figs. 2, 3 and 5). The data showed a positive relationship between T_2 spatial complexity and alpha EEG resonance, at the expense of theta or delta power (Figs. 2, 3 and 5). The second spatial derivative of T_2 relaxation time also acted like a 'spatial lens' or a focusing of the 3-dimensional spatial locations of T_2 , which is significantly correlated to a more spatially localized alpha EEG activity in the posterior cortical regions (Fig. 4). Importantly, the T_2 relaxation yielded 3-dimensional relationships between sub-volumes and the distribution of electrical potentials at the scalp surface, especially in the TBI patients.

Table 4
ANOVA for neuropsychological performance and EEG

| | EEG relative power | | | | EEG CSD | | | |
|-----------------------|--------------------|---------|----------|---------|----------|---------|----------|---------|
| | δ | ϕ | α | β | δ | ϕ | α | β |
| WAIS | -0.0001 | -0.0001 | +0.0001 | +0.0001 | -0.0001 | -0.0001 | +0.0001 | +0.0001 |
| COWA | -0.0001 | -0.0001 | +0.0001 | +0.0001 | -0.0001 | -0.0001 | +0.0001 | +0.0001 |
| Trail making | -0.0001 | +0.0001 | -0.0001 | NS | -0.0061 | +0.0038 | NS | NS |
| WISC card sort | NS | -0.0001 | +0.0001 | NS | NS | -0.0005 | +0.0002 | NS |
| Wechsler memory scale | -0.0001 | -0.0001 | +0.0001 | +0.0001 | -0.0001 | -0.0001 | +0.0001 | +0.0001 |
| CVLT | -0.0001 | NS | +0.0001 | +0.005 | -0.0001 | -0.0313 | +0.0001 | +0.0319 |
| Sternberg | +0.0001 | -0.0001 | NS | NS | +0.017 | NS | NS | NS |
| VSPL | +0.0001 | -0.0001 | -0.0001 | +0.0009 | NS | NS | NS | NS |

The implications are that measures of the EEG at the scalp surface are linearly related to the molecular integrity of neurons located inside sub-volumes of the brain as measured by the MRI. The neuropsychological–cognition

correlations in this study suggest that there is a measurable relationship between the ‘healthy’ resonant frequencies of the EEG and the molecular integrity of the underlying sources of the EEG.

Normals- MRI-T2 Gray Matter with EEG-Relative Power

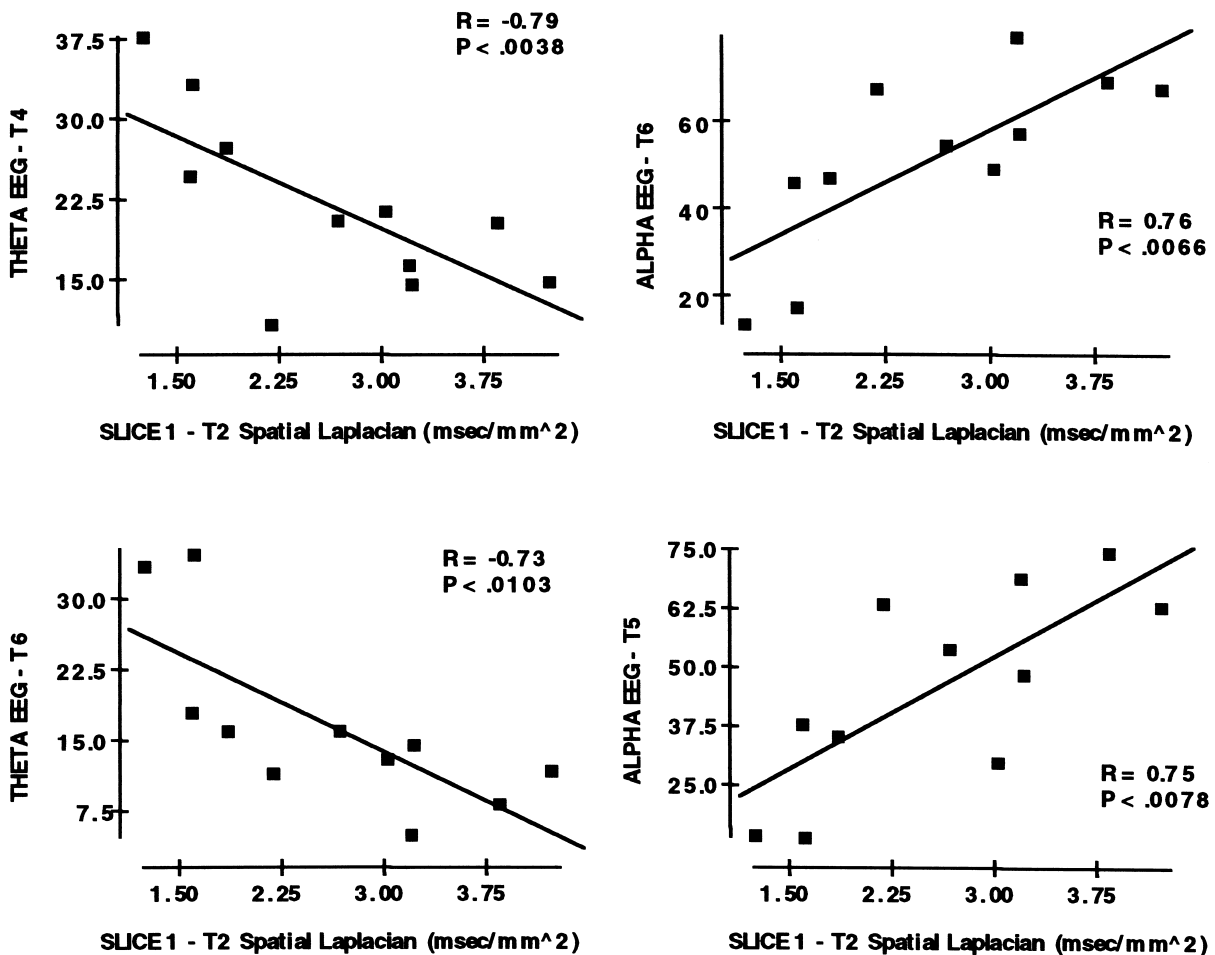


Fig. 6. Correlations between EEG and relaxometry in normal control subjects. The left column are scattergrams between EEG relative power and T_2 relaxation time in the alpha frequency band. The right column are scattergrams between EEG relative power and the spatial Laplacian of T_2 relaxation time in the same EEG leads and the same alpha frequency band as on the right. Similar to the correlations observed in TBI patients (Fig. 3), the normal control subjects also demonstrated opposite directions of correlation between T_2 and the spatial Laplacian of T_2 relaxation time.

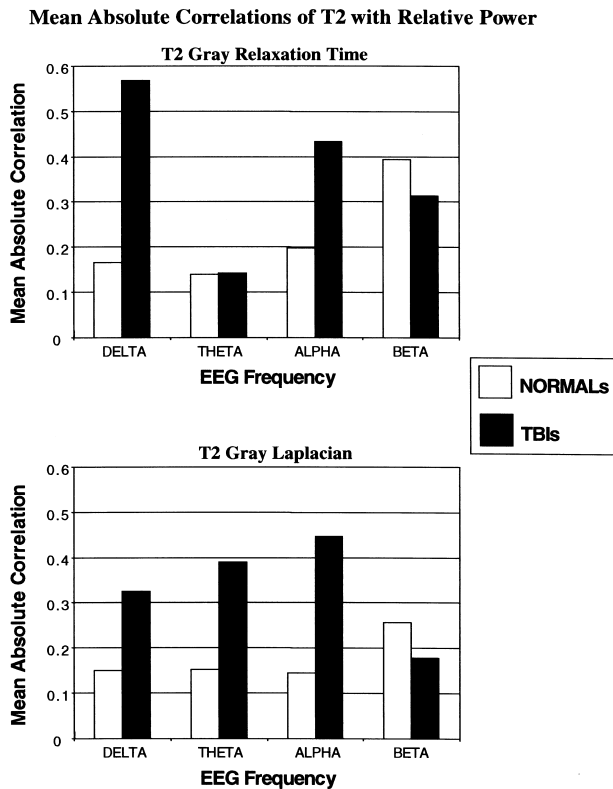


Fig. 7. Relative sensitivity of correlation between EEG and T_2 in normals and TBI patients: (Top) is the mean absolute correlation of T_2 relaxation time with EEG relative power in normal subjects (open columns) and TBI patients (black columns) for the different frequency bands; (Bottom) is the mean absolute correlation of the Laplacian of T_2 relaxation time with EEG relative power in normal subjects (open columns) and TBI patients (black columns) for the different frequency bands.

The observed correlations between relaxometry and qEEG were not significantly related to the age of the patients or the time from injury to EEG and MRI recording. A weaker and more spatially localized EEG correlation was observed in normal control subjects (Figs. 6 and 7).

4.1. Limitations of the study

One limitation of this study is the use of a two-point estimate of T_2 weighted relaxation time. This limitation, however, does not invalidate the statistically significant correlations between T_2 relaxation time and EEG and cognitive functioning. Also, the T_2 relaxation times obtained using a conventional spin-echo method in the present study are markedly similar to other studies using two-point estimates of T_2 (Kirsch et al., 1992; De Certaines et al., 1993) as well as studies using 16-point estimates of T_2 (Rinck, 1993; Laako et al., 1996). Laako et al. (1996) and Kirsch et al. (1992) using 16-point vs. two-point estimates of T_2 , respectively, found very similar results of increased T_2 relaxation related to the clinical severity of dementia. There is considerable consistency in the MRI relaxometry literature in which increased T_2 relaxation times are correlated

with severity of clinical status no matter how many points are used to estimate T_2 (Tillmann et al., 1997; Laako et al., 1996; Kirsch et al., 1992; Miot-Norault et al., 1997).

A limitation of the present study is that T_2 relaxation time is dependent on many factors such as temperature, mobility of observed spin, the presence of large molecules, paramagnetic ions and molecules and field inhomogeneities (Narayana et al., 1988; Dawant et al., 1993). However, we attempted to minimize the biophysical uncertainty by computing the second spatial derivative of T_2 relaxation time or the Laplacian. The spatial Laplacian is not related to the absolute values of T_2 relaxation time itself, rather it is related to the local spatial rate of change in T_2 relaxation time in the local vicinity of each MRI pixel. The spatial Laplacian is also insensitive to B_0 and B_1 magnetic field inhomogeneities since the Laplacian = 0 for global or slow gradient field changes. This study also excluded gray matter regions, which were near to ventricles or sinuses that are the largest sources of MRI field inhomogeneities.

4.2. Spatial heterogeneity of T_2 relaxation time as a measure of entropy

The transverse relaxation time or T_2 of water protons is proportional to the spin homogeneity of the local microenvironment within which a given water proton is located (Wehrli, 1992). Spin homogeneity increases with an increased number of water protons, thus the CSF exhibits long T_2 relaxation times (e.g. >100 ms). Spin homogeneity decreases with macromolecular interactions. For example, the repulsive forces of hydrophobic fat molecules in myelin (e.g. cholesterol, Koenig, 1991) results in a short T_2 relaxation time (e.g. <70 ms). In the gray matter, water protons interact in the homogeneous environment of the hydrophobic and hydrophilic proteins that make up the membranes of neurons, glia and other cellular compartments of the gray matter.

Qualitative terms such as spatial homogeneity vs. inhomogeneity can be more precisely defined using the mathematics of thermodynamics and information theory (Chaitin, 1987; Nicholis and Prigogine, 1989). The assumptions are that T_2 relaxation time is random and linearly related to a thermodynamical order in a voxel as defined by entropy (Feynman et al., 1963, I-47). Based on these assumptions, spatial differences in T_2 relaxation time of neighboring and adjacent voxels of the brain can be defined as a spatial metric of 'information' and 'order' (Chaitin, 1987). According to Poisson's distribution, the probability of one molecule of free water n_i located within a total volume of water ΔV is $P_n = e^{-\bar{n}} (\bar{n}^n / n!)$ where \bar{n} is the mean number of water molecules in the volume (Nicholis and Prigogine, 1989). Given this thermodynamic formulation, the spatial homogeneity of T_2 relaxation time occurs when there is no difference in T_2 relaxation time between two MRI volumes or voxels or when $\Delta T_2 = 0$. According to thermodynamics and information theory, the homogeneous condition is

when the entropy ‘ E ’ of the system is maximum and the spatial Laplacian = 0. This is a state of least order, which is the state of free water in T_2 relaxation time. That is, the change in T_2 with space (t) approaches zero as the amount of free water increases and the macromolecular complexity of the brain decreases. On the other hand, when there are

significant spatial differences in T_2 relaxation time, $T_{2i} - T_{2j} \neq 0$, and entropy decreases proportional to the magnitude of the differences or to the amount of spatial heterogeneity. The Laplacian operator provides a coordinate independent estimate of the spatial ‘homogeneity’ in a T_2 volume and, therefore, it is a metric of the complexity of the

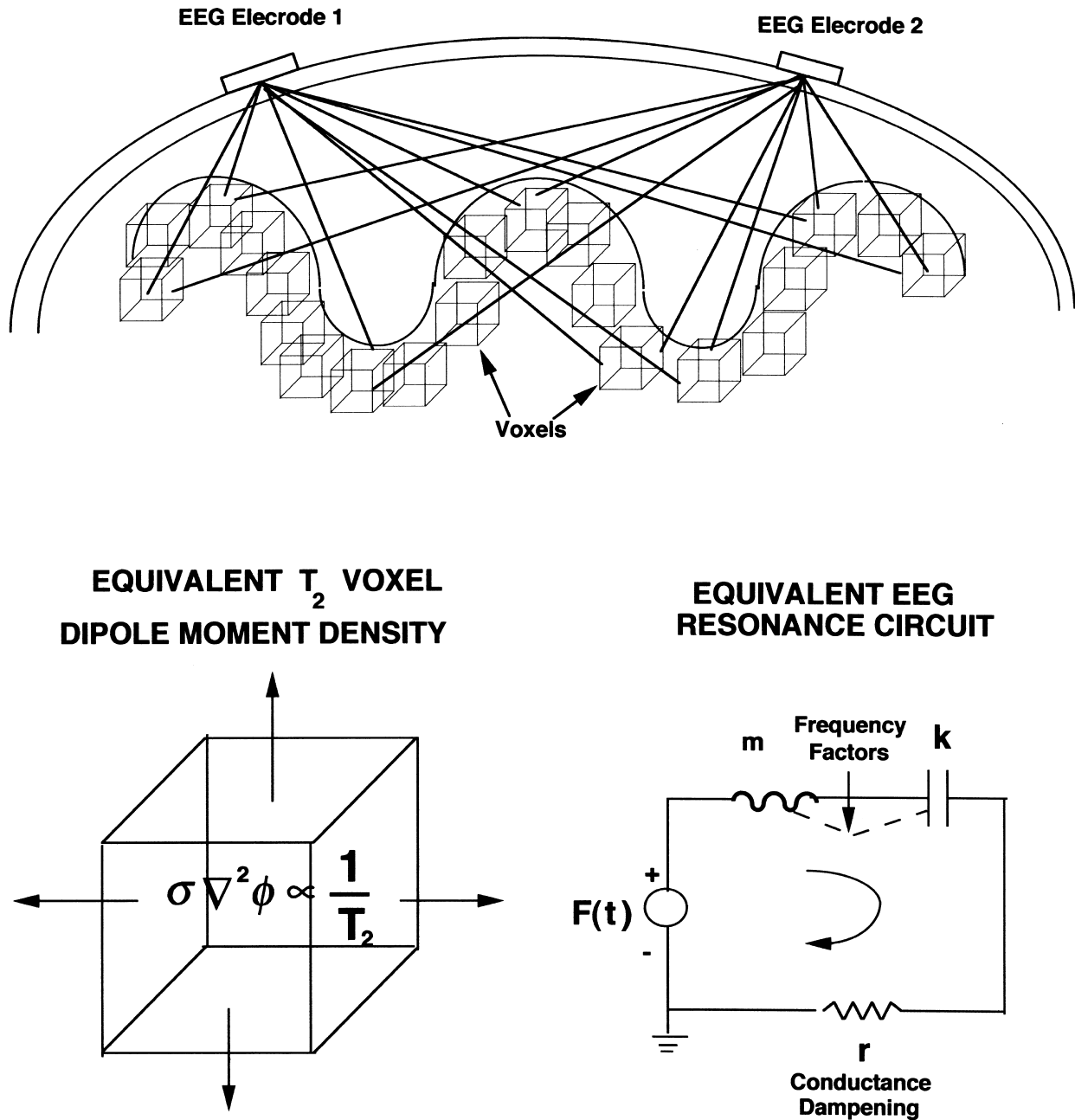


Fig. 8. Diagrammatic model of EEG and MRI linkage. Top is a diagram of the human scalp with two electrodes sensing electrical activity arising from widely distributed volumes or voxels of neocortex. Synaptic and axonal connections between voxels is assumed and each electrode ‘sees’ similar electrical potentials but at different angles and distances. Bottom left is an equivalent T_2 voxel in which the linkage between qEEG and qMRI is the product of the average concentration of ionic channels and the average electrical field which is inversely related to T_2 relaxation time. Bottom right is an equivalent circuit representing a large number of interconnected voxels that resonate by virtue of the synaptic rise times and conduction velocities in the volume as described by Lopes da Silva (1987) and Nunez (1981, 1995). The linkage between qMRI and qEEG is represented by the ‘resistance’ (r) and the Q or quality factor (m and k) which determines the breadth or spread of the resonance. The partial differential equation that is used to model the relationship between qMRI T_2 and the resonant frequencies of the qEEG is Eq. (A4) in Appendix A.

biophysical space. The theoretical advantage of the Laplacian operator, in this study, is coordinate free measures of entropy and biophysical order as it is related to the resonance and power spectrum of the EEG.

4.3. Hypothesized linkage between T_2 relaxation time and EEG (rEEG)

The hypothesized linkage between qMRI and qEEG referred to as relaxometry EEG (rEEG) arises because the membranes of the gray matter of the neocortex contain a large number of ionic channels and ionic pumps in a given volume. It is assumed that a reduced density of neural membranes is linked to lengthened T_2 , which is linked to reduced average current flux produced by ionic channels (e.g. Na^+ , K^+ , Ca^{2+}) in that volume of neocortex. This hypothesis is plausible because only the membranes of neurons in the cortex generate the EEG in the first place (Purpura, 1959; Malmivuo and Plonsey, 1995; Freeman, 1975; Nunez, 1981). As the concentration of ionic channels and/or rate of ionic channel opening decreases, the amplitude of the EEG decreases and there is a shift toward lower frequencies. A reasonable hypothesis is that the attenuation and shift toward lower qEEG frequencies in TBI patients occurs because there are fewer ionic channels and/or more damaged ionic channels per unit volume as correlated with increased T_2 relaxation times.

To understand the hypothesized linkage between qEEG and qMRI, it is important to remember that the concentration of ionic channels and the rate of opening and closing of ionic channels in the cerebral cortex significantly influences the power spectrum of the EEG. In this study, the TBI patients, ranging from mild to severe showed a linear relationship between the qEEG and the qMRI. Linear relationships between qEEG and qMRI in different selections of TBI patients have also been reported (Thatcher et al., 1998a,b). A new contribution of this study is that the resonant frequencies of the EEG appear to be related to the concentration of macromolecules inside the gray matter of the brain. A more detailed explanation is that the transverse relaxation time or T_2 of water protons is proportional to the concentration of macromolecules in a volume of water (Fullerton, 1992; Wehrli, 1992; Bottomley et al., 1984). For example, the CSF is bright in the MRI picture because it is the most homogenous microenvironment with the longest T_2 relaxation times (e.g. 150 ms). The white matter is dark in the T_2 MR image because it contains a high concentration of lipids which are hydrophobic, consequently, T_2 relaxation time is much shorter than CSF (e.g. 60–90 ms). Cortical gray matter does not contain a high concentration of lipids, however, it does contain a high concentration of unmyelinated dendrites, synapses, axons and glial cells and the T_2 relaxation time of gray matter is longer than for white matter but shorter than for CSF (Fullerton, 1992; Wehrli, 1992). In the present study, the segmentation of gray matter MRI pixels was based on a multispectral segmentation (i.e.

T_1 , T_2 and PD) and it is limited to the selection of slices that do not contain sinus cavities and ventricles (Fig. 1). Given these facts, the postulated linkage of T_2 relaxometry to EEG (rEEG) arises because it is reasonable to assume that the number of ionic channels in a volume of neocortex is proportional to the concentration of protein/lipid molecules in that volume (see Appendix A).

4.4. Frequency tuning as a spatial–temporal transfer function between MRI and EEG

The results of this study show frequency tuning in which the alpha frequency band is inversely related to T_2 relaxation time and positively related to the spatial Laplacian and the delta band is positively related to T_2 relaxation time and inversely related to the spatial Laplacian (Fig. 4). The observed relations between T_2 relaxation time and the EEG frequency spectrum in this study are consistent with the transfer function models of EEG by Freeman (1975), Nunez (1981, 1994), Van Rotterdam et al. (1982), Lopes da Silva (1987, 1994) and Pascual-Marqui and Matsinos (1999) for the local and global genesis of the EEG. The new contribution in this study to these models is the addition of a weighting coefficient for the inverse of T_2 relaxation time defined by the Poisson equation as $\mathbf{J}^i = f(1/T_2)$ where \mathbf{J}^i is the volume dipole moment density or source in an unbounded homogeneous volume produced by the membrane ionic flows per time within a voxel of the neocortex (Appendix A).

The mathematical details of a model that relates the EEG power spectrum to the qMRI is shown in Appendix A. Fig. 8 is an equivalent circuit to illustrate the hypothesized inverse relationship between T_2 relaxation time, voxel EEG dipole moment density and the scalp EEG. The top of Fig. 8 illustrates that all EEG scalp electrodes detect the electrical potentials from the same 3-dimensional sources at a given instant of time, but with different amplitudes and angles depending on the locations and magnitudes of the current sources (Malmivuo and Plonsey, 1995). The lower left of Fig. 8 is a model of an equivalent electrical current source in a given voxel and the lower right is the equivalent electrical circuit for large volumes of the neocortex.

The linkage between qMRI and qEEG is represented by the ‘resistance’ (conductivity = 1/resistance), which determines the resonance amplitude and the Q or quality factor which determines the breadth or spread of the resonance.

Fig. 8 shows the linkage between qMRI and qEEG as represented by the ‘resistance’ (inverse of conductivity) which determines the resonance amplitude of the alpha peak and the Q or quality factor which determines the breadth or spread of the resonance. The results of this study indicate that the dampening factor r or resistance is the strongest factor in the relationship between qMRI T_2 and qEEG. Fig. 9 shows the results of the fit of T_2 relaxation time to the transfer function in Appendix A.

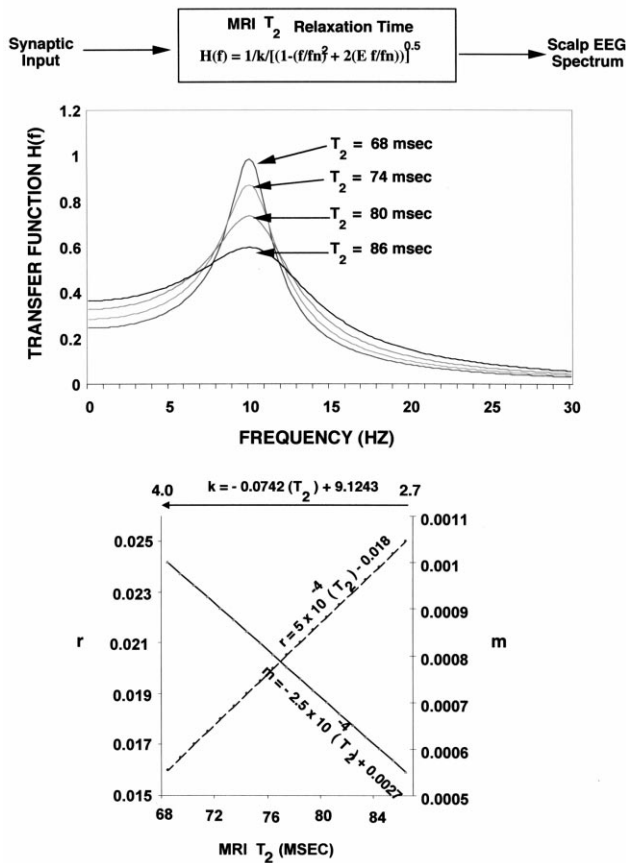


Fig. 9. Linear transfer function model between EEG alpha resonance and T_2 relaxation time. Top shows the linear transfer function (Eq. (A5), Appendix A) to model the relationship between EEG alpha resonance and T_2 relaxation time. The middle is the gain factor of the transfer function $H(f)$ using different values of T_2 relaxation time. The bottom are the linear best fit values for Eqs. (A8a)–(A8c) (Appendix A) or the parameters of the model, which vary as a function of T_2 relaxation time. Eqs. (A8a)–(A8c) (Appendix A) defines the relationship between T_2 and the parameters of the transfer function and an idealized ‘equivalent circuit’ model of the transfer function is in the bottom right of Fig. 8.

5. Conclusions

The general implication of this study is that the average molecular entropy of the brain is related to specific resonant frequencies of the EEG. As the MRI biophysical landscape approaches that of free water or becomes more smooth, the amplitude of alpha EEG resonance decreases and the amplitude of delta activity increases. Another conclusion is that knowledge of the qEEG predicts qMRI and vice versa, knowledge about qMRI predicts the qEEG even though the qMRI and qEEG measurements were taken hours or days apart in time. With improved experimental conditions and improved signal-to-noise measurements, more accurate estimates of physical constants in a qEEG–qMRI transfer function may be estimated, in other populations than TBI patients. The practical use of T_2 derived physical constants or estimates of CSD may be relevant to large volume EEG source localization but it may also be of value in indepen-

dent component analysis (ICA) of the EEG (Makie et al., 1996) in which non-orthogonal and independent global and local resonant frequencies may be correlated with T_2 relaxation time.

The results of this study further validate the usefulness of the qEEG in the evaluation of the severity and extent of TBI by demonstrating a direct linkage at the molecular level of the MRI. The conventional MRI is relatively insensitive to the detection of TBI even in severe TBI (Gentry et al., 1998; Gentry, 1990, 1994). In contrast, qEEG has been shown to be >90% sensitive in the detection of patterns in the EEG in mild TBI (Thatcher et al., 1989, 1991, 2001; Trudeau et al., 1998; Hoffman et al., 1995, 1996; Thornton, 1999). The results of this study suggest that the clinical sensitivity of EEG and MRI may be improved by biophysical linkages and deeper understanding of their common origins.

Acknowledgements

We would like to acknowledge Dr Rex Bierley for discussions of the neuropsychological tests and Ms Kathleen Haedt for administering the neuropsychological tests. We are also indebted to Dr J.C. Daniel for efforts in arranging for the acquisition of MR images in the normal control subjects. This project was supported by contract no. JFC36285006 as part of the Department of Defense and Veterans Head Injury Program (DVHIP). Informed consent was obtained from all subjects in this study.

Appendix A

We assume a volume source in an infinite homogeneous volume conductor in which we define the impressed current density in a voxel as $\mathbf{J}^i(x, y, z, t)$ where \mathbf{J}^i is the individual source element defined as the dipole moment density of the non-conservative current source in a volume (Maliuivuo and Plonsey, 1995, p. 134). Because $\mathbf{J}^i = \mathbf{0}$ outside the boundary of a volume, a partial differential equation referred to as the Poisson equation defines the dipole moment density of a current source inside an unbounded homogeneous volume as:

$$\nabla \cdot \mathbf{J}^i = \sigma \nabla^2 \Phi \tag{A1}$$

where Φ is the electrical potential and σ the conductivity and $\nabla \cdot \mathbf{J}^i$ is referred to as the source or forcing function (Maliuivuo and Plonsey, 1995). The Poisson equation is a differential equation of the 3-dimensional gradient of the electrical potential Φ given the conductivity σ . The net flux of elemental source currents in a bounded volume is 0 but in an unbounded homogeneous volume such as the approximately 3 mm³ MRI volumes in this study, the net flux of individual source currents is $\sigma \nabla^2 \Phi$. The solution of the Poisson equation for the scalar function $\sigma \Phi$ that is uniform and infinite in extent is (Maliuivuo and Plonsey,

1995):

$$4\pi\sigma\Phi = - \int_v (1/r)\nabla\cdot\mathbf{J}^i dv \quad (\text{A2})$$

As described by Malmiuvuo and Plonsey (1995, Eq. (7.4)) the source element $-\nabla\cdot\mathbf{J}^i dv$ in Eq. (A2) behaves like a point source, in that it sets up a field that varies as $1/r$ and is defined as a flow source density for a given volume. A simple rearrangement of Eq. (A2) represents the distribution of electrical potential Φ due to the source \mathbf{J}^i within an infinite, homogeneous volume conductor having conductivity σ that varies as $1/r$ and \mathbf{J}^i is referred to as the volume dipole density (Malmiuvuo and Plonsey, 1995, Eq. (7.5)).

The hypothesized biophysical relationship between EEG dipole source density and T_2 relaxometry is modeled by adding an ionic channel function to the Poisson equation:

$$\sigma\nabla^2\Phi \propto f(1/T_2) \quad (\text{A3})$$

where σ is conductivity and $\nabla^2\phi$ is the squared divergence of the gradient of the electrical potential ϕ in Eqs. (A1) and (A2) and $f(1/T_2)$ is a function of the volume dipole density as a linear estimate of the MRI T_2 relaxation time. The addition in this study to the application of the Poisson equation is a T_2 estimate of the concentration and time derivatives of ionic channels in a given voxel. For the purposes of a transfer function, we define the scalar absolute magnitude of the dipole moment density element for each voxel as $|\mathbf{J}| = (x^2 + y^2 + z^2)^{0.5}$ where x , y , and z are components of the dipole moment vector.

A unitless and reference-free rEEG equation for a given 3 mm^3 voxel or a collection of 3 mm^3 voxels is defined as:

$$F(t) = m(T_2)\frac{\partial^2|\mathbf{J}|}{\partial t^2} + r(T_2)\frac{\partial|\mathbf{J}|}{\partial t} + k(T_2)|\mathbf{J}| \quad (\text{A4})$$

where $F(t)$ is a periodic function of the average synaptic input to a given neocortical voxel at each moment of time, $m(T_2)$ is a function that weights the inertia of the system, $|\mathbf{J}|$ is the absolute magnitude of the dipole moment density in a voxel of neocortex, $r(T_2)$ is a function that weights the dampening of the wave and $k(T_2)$ is a function that weights the frequency response of the system.

The transfer function that relates the EEG output to the average synaptic drives (dipole moment density) in a volume of neocortex or rEEG(t) can be found by setting $F(t) = 0$ and taking the Fourier transform of both sides of Eq. (A4) (Bendat and Piersol, 1980, pp. 62–81):

$$|H(f)| = \frac{1/k}{\sqrt{[1 - (f/f_n)^2]^2 + [2Ef/f_n]^2}} \quad (\text{A5})$$

where $H(f)$ is the transfer function in the frequency domain, f the driving frequency, f_n is the resonance frequency and E the dampening ratio. f_n and E are defined by Bendat and Piersol (1981, p. 83) as:

$$f_n = \frac{1}{2\pi}\sqrt{\frac{k}{m}} \quad (\text{A6})$$

$$E = \frac{r}{2\sqrt{km}} \quad (\text{A7})$$

The influence of T_2 weighted relaxation time on the resonant peak of the EEG alpha frequency was modeled by assuming a linear relationship between qMRI T_2 and the inertia of the system m , the dampening factor r and the factor k in Eq. (A4). Eqs. (A8a)–(A8c) show the straight line fits that were used to estimate values of m , r and k used in Eq. (A4):

$$m = a(1/T_2) + b \quad (\text{A8a})$$

$$r = -d(1/T_2) + e \quad (\text{A8b})$$

$$k = h(1/T_2) + i \quad (\text{A8c})$$

The intercept and range of values for the parameters of the transfer function are shown in the bottom of Fig. 9. The dampening factor r was the most significant parameter that linked the experimental observations to the model.

References

- Advani SH, Ommaya AK, Yang WJ. Head injury mechanisms, characteristics and clinical evaluation. In: Chista D, editor. Human body dynamics, Oxford medical engineering series, Oxford: Clarendon Press, 1982. pp. 3–37.
- Barth J, Macciocchi S, Giordani B. Neuropsychological sequelae of minor head injury. *Neurosurgery* 1983;13:520–537.
- Bendat JS, Piersol AG. Engineering applications of correlation and spectral analysis, New York, NY: Wiley, 1980.
- Bensaid AM, Hall LO, Bezdek JC, Clarke LP. Fuzzy cluster validity in magnetic resonance images. In: Loew MH, editor. Proc SPIE, 1994. pp. 454–464.
- Bezdek JC, Hall LO, Clarke LP. Review of MR image segmentation techniques using pattern recognition. *Med Phys* 1993;20:1033–1048.
- Bloch F. Nuclear induction. *Phys Rev* 1946;70:460–482.
- Bottomley PA, Foster TH, Argersinger RE, Pfeifer LM. A review of normal tissue hydrogen NMR relaxation times and relaxation mechanisms from 1–100 MHz: dependence on tissue type, NMR frequency, temperature, species, excision and age. *Med Phys* 1984;11(4):425–448.
- Chaitin G. Algorithmic information theory. Cambridge University Press, Cambridge, England, 1987.
- Clarke LP, Velthuisen RP, Camacho MA, Heine JJ, Vaidyanathan M, Hall LO, Thatcher RW, Silbiger ML. MRI segmentation: methods and applications. *Magn Reson Imaging* 1995;13:343–368.
- Cronwall D, Wrightson P. Delayed recovery of intellectual function after minor head injury. *Lancet* 1980;11:605–609.
- Daniel JC, Olesiewicz M, Reeves DL, Tam D, Bleiberg J, Thatcher RW, Salazar AM. Repeated measures of cognitive processing efficiency in adolescent athletes: implications for monitoring recovery from concussion. *Neuropsychiatry Neuropsychol Behav Neurol* 1999;12(3):167–169.
- Darwin RH, Drayer BP, Riederer SJ, Wang HZ, MacFall JR. T_2 estimates in healthy and diseased brain tissue: a comparison using various MR pulse sequences. *Radiology* 1986;160:375–381.
- Dawant BM, Zijdenbos AP, Margolin RA. Correction of intensity variations in MR images for computer-aided tissue classification. *IEEE Trans Med Imaging* 1993;12:770–781.

- De Certaines JD, Henriksen O, Spisni A, Cortsen M, Ring IV PB. In vivo measurements of proton relaxation times in human brain, liver, and skeletal muscle: a multicenter MRI study. *Magn Reson Imaging* 1993;11:841–850.
- Dixon RL, Ekstrand KE. The physics of proton NMR. *Med Phys* 1982;9:807–818.
- Freeman WJ. Mass action in the nervous system, New York, NY: Academic Press, 1975.
- Feynman RP, Leighton RB, Sands M. The Feynman lectures on physics, vols. I and II. Reading, MA: Addison-Wesley, 1963.
- Fullerton GD. Physiological basis of magnetic relaxation. In: Stark DD, Bradley WG, editors. *Magnetic resonance imaging*, St. Louis, MO: Mosby, 1992. pp. 88–108 (Mosby year book).
- Gentry LR. Head trauma. In: Atlas SW, editor. *Magnetic resonance imaging of the brain and spine*, New York, NY: Raven Press, 1990. pp. 439–466.
- Gentry LR. Imaging of closed head injury. *Radiology* 1994;191:1–17.
- Gentry LR, Godersky JC, Thompson B. MR imaging of head trauma: review of the distribution and radiopathologic features and traumatic lesions. *Am J Radiol* 1988;150:663–672.
- Hickley DS, Checkley D, Aspden RM, Naughton A, Jenkins JP, Isherwood I. A method for the clinical measurement of relaxation times in magnetic resonance imaging. *Br J Radiol* 1986;59:565–576.
- Hoffman DA, Stockdale S, Hicks L. Diagnosis and treatment of head injury. *J Neurotherapy* 1995;1(1):14–21.
- Hoffman DA, Stockdale S, Van Egren L, et al. Symptom changes in the treatment of mild traumatic brain injury using EEG neurofeedback. *Clin Electroencephalogr (Abstract)* 1996;27(3):164.
- Holbourn AHS. The mechanics of brain injuries. *Br Med Bull* 1945;3:147–149.
- Kirsch SJ, Jacobs RW, Butcher LL, Beatty J. Prolongation of magnetic resonance T_2 time in hippocampus of human patients marks the presence and severity of Alzheimer's disease. *Neurosci Lett* 1992;134:187–190.
- Koenig SH. Cholesterol of myelin is the determinant of gray–white contrast in MRI of brain. *Magn Reson Med* 1991;20:285–291.
- Kjos O, Ehman RL, Brant-Zawadzki M, Kelly WM, Normas D, Newton TH. Reproducibility of relaxation times and spin density calculated from routine MR imaging sequences: clinical study of the CNS. *Am J Radiol* 1985;144:1165–1170.
- Kwentus JA, Hart RP, Peck ET, et al. Psychiatric complications of closed head trauma. *Psychosomatics* 1985;26:8–15.
- Laako MP, Partanen K, Soininen H, Lehtovirta M, Hallikainen M, Hanninen T, Helkala EL, Vaino P, Riekkinen PJ. MR T_2 relaxometry in Alzheimer's disease and age-associated memory impairment. *Neurobiol Aging* 1996;17(4):535–540.
- Lee YC, Advani SH. Transient response of a sphere to symmetric torsional loading: a head injury model. *Math Biosci* 1970;6:473–487.
- Lopes da Silva FH. Dynamics of EEGs as signals of neuronal populations: models and theoretical considerations. In: Niedermeyer E, Lopes da Silva FH, editors. *Electroencephalography*, Baltimore, MD: Williams and Wilkins, 1987.
- Lopes da Silva FH. Dynamics of electrical activity of the brain, Neocortical dynamics and human EEG rhythms. New York, NY: Oxford University Press, 1995.
- Makeig S, Bell AJ, Jung TP, Sejnowski TJ. Independent component analysis of electroencephalographic data. *Adv Neural Information Process Syst* 1996;8:145–151.
- Malmivuo J, Plonsey R. *Bioelectromagnetism*, New York, NY: Oxford University Press, 1995.
- Mas F, Prichep LS, Alper K. Treatment resistant depression in a case of minor head injury: an electrophysiological hypothesis. *Clin Electroencephalogr* 1993;24(3):118–122.
- Mills CM, Crooks LE, Kaufman L, Brant-Zawadzki M. Cerebral abnormalities: use of calculated T_1 and T_2 magnetic resonance images for diagnosis. *Radiology* 1984;150:87–94.
- Miot-Noirault E, Barantin L, Akoka S, Le Pape A. T_2 relaxation time as a marker of brain myelination: experimental MR study in two neonatal animal models. *J Neurosci Methods* 1997;72:5–14.
- Narayana PA, Brey WW, Kulkarni MV, Sievenpiper CL. Compensation for surface coil sensitivity variation in magnetic resonance imaging. *Magn Reson Imaging* 1988;6(3):271–274.
- Nicholis G, Prigogine I. *Exploring Complexity*, W.H. Freeman and Co., New York, 1989.
- Nunez P. *Electrical fields of the brain*, Cambridge, MA: Oxford University Press, 1981.
- Nunez P. *Neocortical dynamics and human EEG rhythms*, New York, NY: Oxford University Press, 1995.
- Ommaya AK. The mechanical properties of tissues of the nervous system. *J Biomech* 1968;2:1–12.
- Ommaya AK. Head injury mechanisms and the concept of preventive management: a review and critical synthesis. *J Neurotrauma* 1995;12(4):527–546.
- Ommaya AK, Thibault LE, Bandak FA. Mechanisms of impact head injury. *Int J Impact Eng* 1994;15(4):535–560.
- Otnes RK, Enochson L. *Digital time series analysis*, New York, NY: Wiley, 1972.
- Pascual-Marqui RD, Matsinos E. Functional mapping with electric brain wave imaging. *NeuroImage* 1999;9(6):S204.
- Pascual-Marqui RD, Gonzalez-Andino SL, Valdes-Sosa PA, Biscay-Lirio R. Current source density estimation and interpolation based on the spherical harmonic Fourier expansion. *Int J Neurosci* 1988;43:237–249.
- Povlishock JT, Coburn TH. Morphopathological change associated with mild head injury. In: Levin HS, Eisenberg HM, editors. *Mild head injury*, New York, NY: Oxford University Press, 1989. pp. 37–53.
- Press WH, Teukolsky SA, Vetterling WT, Flannery BP. *Numerical recipes in C*, Cambridge, MA: Cambridge University Press, 1994.
- Purpura DP. Nature of electrocortical potentials and synaptic organizations in cerebral and cerebellar cortex. In: Pfeiffer CC, Smythies JR, editors. *International review of neurobiology*, vol. I. New York, NY: Academic Press, 1959.
- Rimel R, Hiodani B, Barth J, Boll T, Jane J. Disability caused by minor head injury. *Neurosurgery* 1981;9:221–223.
- Ruijs MB, Gabreels FJ, Thijssen HM. The utility of electroencephalography and cerebral computed tomography in children with mild and moderately severe closed head injuries. *Neuropediatrics* 1994;25(2):73–77.
- Savitzky A, Golay MJE. Smoothing and differentiation of data by simplified least squares procedures. *Anal Chem* 1964;36:1627–1639.
- Tebano MT, Cameroni M, Gallozzi G, Loizzo A, Palazzino G, Pezzino G, Pezzini G, Ricci GF. EEG spectral analysis after minor head injury in man. *EEG Clin Neurophysiol* 1988;70:185–189.
- Thatcher RW, Walker RA, Gerson I, Geisler F. EEG discriminant analyses of mild head trauma. *EEG Clin Neurophysiol* 1989;73:93–106.
- Thatcher RW, Cantor DS, McAlaster R, Geisler F, Krause P. Comprehensive predictions of outcome in closed head injury: the development of prognostic equations. *Ann NY Acad Sci* 1991;620:82–104.
- Thatcher RW, Camacho M, Salazar A, Linden C, Biver C, Clarke L. Quantitative MRI of the gray–white matter distribution in traumatic brain injury. *J Neurotrauma* 1997;14:1–14.
- Thatcher RW, Biver C, Camacho M, McAlaster R, Salazar AM. Biophysical linkage between MRI and EEG amplitude in closed head injury. *NeuroImage* 1998a;7(4):352–367.
- Thatcher RW, Biver C, McAlaster R, Salazar AM. Biophysical linkage between MRI and EEG coherence in traumatic brain injury. *NeuroImage* 1998b;8(4):307–326.
- Thatcher RW, Biver CJF, Gomez M, Salazar AM. 3-Dimensional vector analysis of MRI relaxometry and current source localization (LORETA) of EEG in traumatic brain injury. *NeuroImage* 2000;9(6):S110.
- Thatcher RW, North D, Curtin R, Walker RA, Biver CJF, Gomez M, Salazar A. An EEG severity index of traumatic brain injury. *J Neuropsychiatry Clin Neurosci* 2001;13(1):77–87.
- Thornton K. Exploratory investigation into mild brain injury and discrimi-

- nant analysis with high frequency bands (32–64 Hz). *Brain Inj* 1999;13(7):477–488.
- Tillman S, Hofmann E, Warmuth-Metz M, Franzek E, Becker T. MRI T_2 relaxation times of brain regions in schizophrenic patients and control subjects. *Psychiatr Res: Neuroimaging Sect* 1997;75:173–182.
- Trudeau DL, Anderson J, Hansen LM, Shagalov DN, Schmoller J, Nugent S, Barton S. Findings of mild traumatic brain injury in combat veterans with PTSD and a history of blast concussion. *J Neuropsychiatry Clin Neurosci* 1998;10(3):308–313.
- Van Rotterdam A, Lopes da Silva FH, van den Ende J, Viergever MA, Hermans AJ. A model of the spatial–temporal characteristics of the alpha rhythm. *Bull Math Biol* 1982;44:283–305.
- von Bierbrauer A, Weissenborn K, Hinrichs H, Scholz M, Kunkel H. Automatic (computer-assisted) EEG analysis in comparison with visual EEG analysis in patients following minor cranio-cerebral trauma (a follow-up study). *EEG EMG Z Elektroenzephalogr Elektromyogr Verwandte Geb* 1993;23(3):151–157.
- Wehrli FW. Principles of magnetic resonance. In: Stark DD, Bradley WG, editors. *Magnetic resonance imaging*, St. Louis, MO: Mosby, 1992. pp. 3–20 (Mosby year book).
- Whittall KP, MacKay AL, Graeb DA, Nugent RA, Li DKB, Paty DW. In vivo measurement of T_2 distributions and water contents in normal human brain. *Mag Reson In Med* 1997;37:34–43.